Triggered reversible disassembly of an engineered protein nanocage

Jesse A. Jones[a], **Ajitha S. Cristie-David**[a], **Michael P. Andreas**[a], **Tobias W. Giessen Prof.**[a,b]

[a]Department of Biomedical Engineering, University of Michigan Medical School, Ann Arbor, 1150 W. Medical Center Dr., MSRB2 Ann Arbor, MI, 48109-5622, USA

[b]Department of Biological Chemistry, University of Michigan Medical School, Ann Arbor, 1150 W. Medical Center Dr., MSRB2 Ann Arbor, MI, 48109-5622, USA

Abstract

Protein nanocages play crucial roles in sub-cellular compartmentalization and spatial control in all domains of life and have been used as biomolecular tools for applications in biocatalysis, drug delivery, and bionanotechnology. The ability to control their assembly state under physiological conditions would further expand their practical utility. To gain such control, we introduced a peptide capable of triggering conformational change at a key structural position in the largest known encapsulin nanocompartment. We report the structure of the resulting engineered nanocage and demonstrate its ability to disassemble and reassemble on demand under physiological conditions. We demonstrate its capacity for *in vivo* encapsulation of proteins of choice while also demonstrating *in vitro* cargo loading capabilities. Our results represent a functionally robust addition to the nanocage toolbox and a novel approach for controlling protein nanocage disassembly and reassembly under mild conditions.
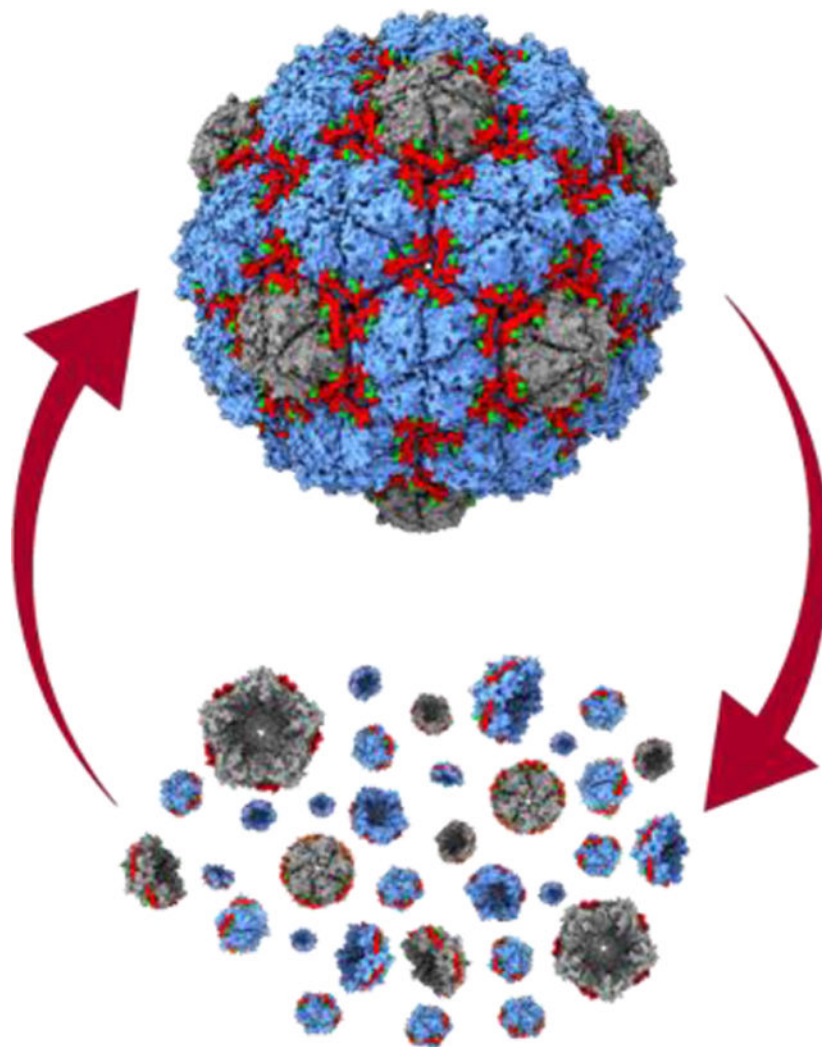
Graphical Abstract

tgiessen@umich.edu .

A novel protein nanocage has been developed capable of on-demand reversible disassembly via simple buffer exchanges under mild conditions. Data presented herein also shows the nanocage is capable of *in vivo* and *in vitro* cargo loading, suggesting a broad range of possible applications in biocatalysis, bionanotechnology and biomedicine. Additional findings include structure determination and protein design verification via cryo-electron microscopy.

Keywords

Intracellular compartmentalization is an effective strategy employed by all organisms to regulate metabolism and achieve spatial control.[1] One widespread compartmentalization approach is the use of protein nanocages. They can accumulate and store labile compounds, sequester toxic or volatile reaction intermediates, and prevent undesired side reactions of encapsulated enzymes.[1] Pioneering efforts have been undertaken to engineer protein nanocages like ferritins, lumazine synthase, and virus-like particles for various biomedical

and industrial applications.[2] Such recent efforts of note include introducing enzyme encapsulation capabilities to ferritin cages[3] and engineered protein shells,[4] as well as the construction of stable artificial protein cages capable of metal-coordinated reversible disassembly.[5] Additional focus on combining these attributes of cargo loading with input-responsive nanostructures capable of triggered assembly or disassembly would prove highly valuable.[6, 7] Such controllable structures could expand the potential application range of engineered nanocages to include programmable delivery of encapsulated payloads and rationally timed substrate-product release and intermixing, to name only a few examples. Encapsulin nanocompartments have recently emerged as a particularly versatile bioengineering tool, resulting in their application as bionanoreactors, targeted delivery systems, and nano- and biomaterials production platforms.[8, 9]

Encapsulins are icosahedral protein nanocages found in bacteria and archaea with triangulation numbers of T=1 (24 nm), T=3 (32 nm) or T=4 (42 nm) containing sub-nanometer pores at the symmetry axes.[10] They self-assemble from a single HK97-fold capsid protein into 60mer (T=1), 180mer (T=3) or 240mer (T=4) protein cages and are involved in oxidative stress resistance,[11-13] iron mineralization and storage,[14, 15] and sulfur metabolism.[16] Their defining feature is the ability to encapsulate dedicated cargo proteins via short C-terminal targeting peptides (TPs) found in cargo proteins which specifically interact with the interior of the protein shell during self-assembly.[13, 17] This native feature has been reliably coopted for the facile encapsulation of non-native proteins through TP-fusions.[18, 19]

Once assembled, encapsulins exhibit notable robustness and stability.[20, 21] While often a desirable characteristic, this also precludes their easy disassembly under physiological conditions, a key feature for responsive delivery systems, nanoreactors, and biomaterials. In particular, encapsulins' inherent stability prevents efficient release of molecules synthesized in their interior, cargo enzyme "hot-swapping" for sequential packaging, or triggered cargo release for drug delivery applications.

Here we develop an engineered protein nanocage based on a bacterial encapsulin that exhibits triggered reversible disassembly under physiological conditions while also maintaining cargo loading capabilities.

Results and Discussion

Protein cage selection and design of the disassembly trigger.

The T=4 *Quasibacillus thermotolerans* encapsulin (QtEnc) was chosen as an engineering scaffold. QtEnc is the largest bacterial encapsulin known to date and is comprised of a thermostable, non-covalent chainmail formed from a single self-assembling protomer. Additionally, QtEnc is easily overexpressed and purified from *Escherichia coli* in an empty or cargo-loaded state.[15] QtEnc was analyzed for engineerable features important for protein cage assembly that might also be tolerant to mutation and would not interfere with cargo loading. Based on previous structural studies, we chose to focus on the elongated loop (loop) region of the encapsulin protein which makes critical intra-and inter-capsomer contacts and influences overall shell topology (Figure 1A).[15, 20, 22] The E-loop is also located away

from the terminal helix important for cargo loading.[23] Therefore, the E-loop was selected as the insertion site for the disassembly trigger.

The GALA peptide has been shown to demonstrate an inducible coil-to-helix conformational change upon acidification[6, 24] and was chosen as a disassembly trigger. A 16-residue GALA peptide flanked by triple glycine linkers was inserted between QtEnc residues Glu61 and Ala62 yielding the engineered nanocage T4GALA (Figure 1B; Figure S1, TableS1). We hypothesized that under neutral and basic conditions, the GALA peptide random coil would not disturb E-loop conformation or shell assembly. Upon acidification, the GALA coil would be expected to adopt a helical conformation and introduce enough torsional strain to disrupt critical E-loop contacts, thereby perturbing structural integrity enough to induce disassembly of the protein cage. A reversion of the GALA helix back to its relaxed random coil state under less acidic conditions would be expected to allow reassembly of the encapsulin cage.

Assembly, disassembly, and reassembly of T4GALA.

To characterize the engineered nanocage, C-terminally His-tagged T4GALA was expressed and purified using Ni-NTA resin and found to still assemble via transmission electron microscopy (TEM) analysis (Figure 2A). Native polyacrylamide gel electrophoresis (PAGE) and preliminary TEM studies were then conducted to analyze the effects of pH, salt, and buffer on the engineered protein cage (Figure S2, Figure S3). T4GALA exhibited a tendency for disassembly at low pH, with near-complete disassembly achieved at pH 6.0, and early TEM analyses showed T4GALA to be capable of disassembling at pH 5.5 and reassembling at pH 7.5 under high imidazole conditions (Figure S3). However, further studies were conducted to discern any potential trigger conditions more amicable to physiological studies. An unexpected dependence of T4GALA structural integrity on buffer identity was subsequently observed. Specifically, it was noted that disassembly at physiological pH was favored in the presence of Tris buffer (pH 7.5) while Bis-tris propane was found to significantly stabilize T4GALA under similar pH conditions.

Size exclusion chromatography (SEC) showed that the elevated imidazole concentrations used for Ni-NTA elution helped maintain T4GALA in an assembled state even in Tris buffer. Imidazole was added to SEC buffers for all subsequent purifications (Figure S4). As such, T4GALA is easily overexpressed in *E. coli* and purified in the assembled state via a simple two-step protocol.

As concern existed regarding the potential for prolonged exposure to Tris buffer and unfavorable pH conditions during native PAGE analysis, assembly states were verified and characterized by a more reliable combination of dynamic light scattering (DLS) analysis and TEM (Figure 2, Figure S5). A streamlined protocol was developed to purify T4GALA via standard Ni-NTA conditions, disassembly in imidazole-free Tris buffer, and reassembly in Bis-tris propane, all under physiological pH conditions. Overall, assembled T4GALA proved to be similar to native QtEnc in size (QtEnc Z-average diameter 47.2 nm, peak diameter 43.4 nm; T4GALA Z-average diameter 62.2 nm, peak diameter 56.39 nm) and monodisperse (Figure 2A), with the slight increase in average diameter by DLS possibly due to the additional disordered insert and potential small lipophilic aggregates. After brief

centrifugation, the disassembled sample appears monodisperse with a diameter of ~6 nm (Z-average diameter 6.8 nm, peak diameter 5.4 nm) (Figure 2B). Upon reassembly, T4GALA re-forms mostly monodisperse protein cages of the expected diameter (Z-average diameter 76.78 nm, peak diameter 55.31 nm), with an increase in aggregation observed by TEM and DLS analysis. (Figure 2C).

Structural characterization of the T4GALA protein nanocage.

To further characterize T4GALA, cryogenic electron microscopy (cryo-EM) was carried out on the engineered protein cage and the structure was determined to 3.57 Å resolution. The overall structure of T4GALA shows that it self-assembles into a 7.7 MDa 240mer (T=4) nanocompartment about 42 nm in diameter, nearly identical to native QtEnc (PDB 6NJ8). However, T4GALA exhibits a notable absence of cryo-EM density in the E-loop region between residues Glu58 and Gly83, corresponding to the GALA insertion site (Figure 3, Figure S6, Figure S7, Table S2). Specifically, E-loops at the three-fold symmetry axis formed by three neighboring hexameric capsomers show no density for 21 out of 22 GALA insertion residues – including the glycine linkers. Three additional residues (Glu58, Ser59, and His60) preceding the GALA insertion site lack density as well. At the pseudo-three-fold axis formed by two hexameric and one pentameric capsomer, a similar absence of density is observed around the GALA insertion site (Figure S8). While density is visible for all other E-loop residues, model-to-map correlation is relatively low for these E-loop residues across different chains (Figure S9), suggesting the engineered E-loop is more structurally dynamic, corroborating the goal of creating a less structurally rigid, triggerable E-loop.

In vivo cargo loading of T4GALA, cargo sequestration, and cargo activity.

An N-terminus SUMO-fused tandem quadruple repeat of split fluorescent protein (sFP) was fused at the C-terminus to a QtEnc targeting peptide (T4TP) and cloned immediately upstream of the T4GALA gene for co-expression (Figure 4A).[15, 25] Addition of the SUMO fusion partner was included to facilitate expression, solubility, and overall ease of use.[26] *In vivo* cargo loading capabilities were then confirmed via Ni-NTA affinity co-purification (Figure 4B). Additionally, plate-based sFP complementation fluorescence analysis further confirmed *in vivo* cargo loading while also confirming triggered disassembly capabilities (Figure 4A, 4B).[27] Assembled $GFP11\times_4$-loaded and disassembled $GFP11\times_4$-bound T4GALA were individually mixed with separately purified GFP1–10 sFP complement and each separate reaction was allowed to mature overnight for 16 hours. Assembled T4GALA prevented the encapsulated $GFP11\times_4$ from interacting with GFP1–10 resulting in low relative fluorescence as compared to disassembled T4GALA, which allowed for robust GFP1–10 complementation yielding more than four-fold relative fluorescence. The ability of T4GALA to create a sequestered nanoscale space and robustly encapsulate its cargo until purposefully triggering disassembly will be a useful feature for various biomolecular engineering applications.

To expand the characterization of *in vivo* loading to enzymes and test potential diffusion barrier effects of encapsulation, a T4 targeting peptide was fused to the C-terminus of a flavin adenine dinucleotide-dependent glucose dehydrogenase enzyme (GDH),[28] cloned immediately upstream of T4GALA, and co-expressed for *in vivo* encapsulation. Cargo

loading capabilities were again confirmed via Ni-NTA affinity co-purification and kinetic analyses were conducted via the 2,6-dichloroindophenol (DCIP) assay, which monitors the decrease in absorbance at 600 nm as DCIP is reduced, to determine whether GDH loaded into T4GALA *in vivo* could maintain enzymatic activity (Table 1, Figure 4C and 4D).[28, 29] Comparisons were therefore made between equimolar amounts of free GDH enzyme, encapsulated GDH, and GDH enzyme bound to disassembled T4GALA. While T4GALA-encapsulated GDH exhibited enzymatic activity with a V_{max} of 0.47 μM/sec (95% CI = 0.42–0.52) in the assembled state and 0.53 μM/sec (95% CI = 0.50–0.56) in the disassembled state, the free enzyme displayed substantially faster kinetics than both encapsulin-bound samples with a V_{max} of 0.77 μM/sec (95% CI = 0.72–0.82). In this case, such results suggest the relative decrease in kinetics to be caused more by the enzyme being bound and encumbered by the encapsulin rather than the encapsulin acting as a barrier to the relatively small glucose substrate. It is widely documented throughout the literature that enzymes tethered to a surface often display decreased specific activity,[30] and it has been further reported that encapsulated enzymes often exhibit decreased specific activity, hypothesized to be the result of rapid *in vivo* encapsulation which may prevent proper folding and cofactor binding.[31]

Additionally, the protein shell likely acts as a diffusion barrier which may decrease the flux of certain larger substrates and products in and out of the protein nanocage. Therefore, a decrease in encapsulated enzyme activity such as that observed here is not wholly unanticipated. Furthermore, kinetic analyses reported from the literature have shown that K_m shows little overall variation upon enzyme encapsulation.[32] Similar findings are observed here with a free GDH enzyme K_m^{app} of 27.68 mM (95% CI = 22.56–33.98) as compared to the T4GALA-encapsulated K_m^{app} of 19.83 mM (95% CI = 13.63–28.71) in the assembled state and 15.16 mM (95% CI = 12.81–18.63) in the disassembled state. Overall, the *in vivo* encapsulation of an active enzyme, along with its maintained activity after disassembly, highlights the potential modularity and applicability of the T4GALA system.

In vitro cargo loading of T4GALA.

To analyze whether the engineered T4GALA protein cage is capable of being disassembled, loaded *in vitro* with exogenous cargo, and then reassembled, a T4 targeting peptide was fused to the C-terminus of mNeonGreen fluorescent protein (mNeonTP). After disassembly of T4GALA, it was mixed with the separately expressed and purified mNeonTP in different molar ratios (6:2 and 6:1 T4GALA:mNeonTP) and then incubated overnight to allow complementation and fluorescent maturation (Figure 5A). Next, T4GALA was reassembled and assessed for *in vitro* cargo loading via native PAGE and SEC via fluorescence analysis, as well as TEM analysis (Figure 5, Figure S10). Fluorescence of the loaded mNeonTP was observed along with the high molecular weight reassembled T4GALA protein band, suggesting the engineered protein cage is capable of being loaded with exogenous cargo *in vitro*. Importantly, the experiment was conducted in parallel with an alternative mCherry fluorescent protein lacking the T4 targeting peptide as a negative control. The negative control sample failed to exhibit *in vitro* T4GALA encapsulation, indicated by a lack of co-migrating fluorescence during native PAGE analysis. The ability to easily encapsulate

proteins inside a defined protein shell under mild conditions *in vitro* once again highlights the potential broad application range of the T4GALA system.

Conclusion

From bionanoreactors to nanotherapeutic technologies, protein nanocage design presents significant opportunities across numerous research fields. While *de novo* protein cage design has led to the addition of remarkable novel biomolecular tools,[33] increasing numbers of natural protein nanocompartments are being discovered that are amenable to rational engineering approaches and add to the biomolecular toolbox.[15, 34] The recent surge in encapsulin nanocompartment discovery and engineering further emphasizes this point.[9, 12, 19, 35] Newly discovered protein cages provide an opportunity to create novel semi-synthetic hybrid compartments and bionanotechnological tools. For example, previous research has shown that disassembling and reassembling viral capsids or encapsulins requires relatively harsh adjustments to pH[7, 36] or salt concentration.[37] In contrast, the T4GALA system described here is functional under milder conditions that may be better suited for conventional experimental procedures and potential biocatalysis or delivery applications than some of the alternative engineered protein cages. The T4GALA nanocage merits further investigation as it exemplifies the potential to add a novel dimension of control to encapsulin nanocages.

Via simple buffer exchanges within physiological pH and ionic strength ranges, the T4GALA system showcases the ability to undergo on-demand disassembly and at least partial reassembly. Regarding the ability of tris buffer to behave as a T4GALA disassembly trigger, it is hypothesized that the biochemical nature of the GALA peptide is responsible. At neutral pH and in the absence of tris (pKa 8.1), Glu residues are negatively charged. The resulting electrostatic repulsions are presumed to destabilize the GALA helix and result in a disordered loop state,[38] allowing the E-loop to behave normally and the T4GALA nanocage to assemble. Upon addition of tris, the charged reactive primary amine may neutralize the charged carboxylic acid moieties of the Glu residues via bridging interactions and promote GALA helix formation, subsequently resulting in T4GALA disassembly. Imidazole (pKa 6.8) may simply act by increasing the buffering capacity, thereby interfering with the above acid-base interactions and allowing T4GALA to assemble. Structural analyses via cryo-EM potentially confirm our overall design strategy by highlighting a lack of density for the rationally engineered disassembly trigger and an altogether more dynamic E-loop.

The engineered protein cage also retains the ability of *in vivo* cargo loading via co-expression with targeting peptide-fused proteins of choice. Additionally, facile *in vitro* cargo loading under mild conditions represents a novel capability for encapsulin nanocages. Potential applications of the T4GALA system include control over the unloading of relatively large encapsulated nanoreactor products, sequentially timed exposure of protected cargos to external molecules, *in vitro* encapsulation of enzymes that cannot be co-expressed with T4GALA, or even stoichiometric shuffling of nanocage components. In sum, the T4GALA system developed here represents a versatile addition to the growing encapsulin-based biomolecular engineering toolbox.

Author Manuscript

Supplementary Material

Refer to Web version on PubMed Central for supplementary material.

Acknowledgements

References

[1]. Cornejo E, Abreu N, Komeili A, Curr. Opin. Cell Biol. 2014, 26, 132–138; Y. Diekmann, J. B. Pereira-Leal, Biochem. J. 2013, 449, 319–331. [PubMed: 24440431]

[2]. Azuma Y, Edwardson TGW, Hilvert D, Chem. Soc. Rev. 2018, 47, 3543–3557; M. Khoshnejad, H. Parhiz, V. V. Shuvaev, I. J. Dmochowski, V. R. Muzykantov, J Control Release 2018, 282, 13–24; Y. Ma, R. J. Nolte, J. J. Cornelissen, Adv. Drug Deliv. Rev. 2012, 64, 811–825; W. F. Rurup, J. Snijder, M. S. Koay, A. J. Heck, J. J. Cornelissen, J. Am. Chem. Soc. 2014, 136, 3828–3832; Y. Azuma, M. Herger, D. Hilvert, J. Am. Chem. Soc. 2018, 140, 558–561; T. G. W. Edwardson, D. Hilvert, J. Am. Chem. Soc. 2019, 141, 9432–9443; E. Sasaki, D. Böhringer, M. van de Waterbeemd, M. Leibundgut, R. Zschoche, A. J. Heck, N. Ban, D. Hilvert, Nat. Commun. 2017, 8, 14663. [PubMed: 29714396]

[3]. Tetter S, Hilvert D, Angew. Chem. Int. Ed. Engl. 2017, 56, 14933–14936. [PubMed: 28902449]

[4]. Zschoche R, Hilvert D, J. Am. Chem. Soc. 2015, 137, 16121–16132. [PubMed: 26637019]

[5]. Malay AD, Miyazaki N, Biela A, Chakraborti S, Majsterkiewicz K, Stupka I, Kaplan CS, Kowalczyk A, Piette BMAG, Hochberg GKA, Wu D, Wrobel TP, Fineberg A, Kushwah MS, Kelemen M, Vavpeti P, Pelicon P, Kukura P, Benesch JLP, Iwasaki K, Heddle JG, Nature 2019, 569, 438–442; E. Golub, R. H. Subramanian, J. Esselborn, R. G. Alberstein, J. B. Bailey, J. A. Chiong, X. Yan, T. Booth, T. S. Baker, F. A. Tezcan, Nature 2020, 578, 172–176. [PubMed: 31068697]

[6]. Choi SH, Choi K, Chan Kwon I, Ahn HJ, Biomaterials 2010, 31, 5191–5198. [PubMed: 20359742]

[7]. Li Y, Conway JF, Cheng N, Steven AC, Hendrix RW, Duda RL, J. Mol. Biol. 2005, 348, 167–182. [PubMed: 15808861]

[8]. Bae Y, Kim GJ, Kim H, Park SG, Jung HS, Kang S, Biomacromolecules 2018, 19, 2896–2904; P. Lagoutte, C. Mignon, G. Stadthagen, S. Potisopon, S. Donnat, J. Mast, A. Lugari, B. Werle, Vaccine 2018, 36, 3622–3628; L. Adamson, N. Tasneem, M. P. Andreas, W. Close, T. N. Szyszka, E. Jenner, R. Young, L. C. Cheah, A. Norman, F. Sainsbury, T. W. Giessen, Y. H. Lau, BioRxiv 2021. [PubMed: 29847113]

[9]. Williams EM, Jung SM, Coffman JL, Lutz S, ACS Synth. Biol. 2018, 7, 2514–2517. [PubMed: 30376298]

[10]. Andreas MP, Giessen TW, Nat. Commun. 2021, 12, 4748. [PubMed: 34362927]

[11]. Lien KA, Nichols RJ, Cassidy-Amstutz C, Dinshaw K, Knight M, Singh R, Eltis LD, Savage DF, Stanley SA, bioRxiv 2020, 2020.2008.2031.276014; C. A. McHugh, J. Fontana, D. Nemecek, N. Cheng, A. A. Aksyuk, J. B. Heymann, D. C. Winkler, A. S. Lam, J. S. Wall, A. C. Steven, E. Hoiczyk, EMBO J. 2014, 33, 1896–1911.

[12]. Giessen TW, Silver PA, Nat. Microbiol. 2017, 2, 17029. [PubMed: 28263314]

[13]. Contreras H, Joens MS, McMath LM, Le VP, Tullius MV, Kimmey JM, Bionghi N, Horwitz MA, Fitzpatrick JA, Goulding CW, J. Biol. Chem. 2014, 289, 18279–18289. [PubMed: 24855650]

Author Manuscript Author Manuscript Author Manuscript Author Manuscript

[14]. He D, Piergentili C, Ross J, Tarrant E, Tuck LR, Mackay CL, McIver Z, Waldron KJ, Clarke DJ, Marles-Wright J, Biochem. J. 2019, 476, 975–989. [PubMed: 30837306]

[15]. Giessen TW, Orlando BJ, Verdegaal AA, Chambers MG, Gardener J, Bell DC, Birrane G, Liao M, Silver PA, Elife 2019, 8.

[16]. Nichols RJ, LaFrance B, Phillips NR, Radford DR, Oltrogge LM, Valentin-Alvarado LE, Bischoff AJ, Nogales E, Savage DF, Elife 2021, 10.

[17]. Akita F, Chong KT, Tanaka H, Yamashita E, Miyazaki N, Nakaishi Y, Suzuki M, Namba K, Ono Y, Tsukihara T, Nakagawa A, J Mol Biol 2007, 368, 1469–1483; W. J. Altenburg, N. Rollins, P. A. Silver, T. W. Giessen, Sci. Rep. 2021, 11, 4951; J. Snijder, O. Kononova, I. M. Barbu, C. Uetrecht, W. F. Rurup, R. J. Burnley, M. S. Koay, J. J. Cornelissen, W. H. Roos, V. Barsegov, G. J. Wuite, A. J. Heck, Biomacromolecules 2016, 17, 2522–2529. [PubMed: 17397865]

[18]. Lau YH, Giessen TW, Altenburg WJ, Silver PA, Nat. Commun. 2018, 9, 1311; M. C. Jenkins, S. Lutz, ACS Synth. Biol. 2021, 10, 857–869. [PubMed: 29615617]

[19]. Sigmund F, Massner C, Erdmann P, Stelzl A, Rolbieski H, Desai M, Bricault S, Wörner TP, Snijder J, Geerlof A, Fuchs H, Hrabě de Angelis M, Heck AJR, Jasanoff A, Ntziachristos V, Plitzko J, Westmeyer GG, Nat. Commun. 2018, 9, 1990. [PubMed: 29777103]

[20]. Tso DJ, Hendrix RW, Duda RL, J. Mol. Biol. 2014, 426, 2112–2129. [PubMed: 24657766]

[21]. Künzle M, Mangler J, Lach M, Beck T, Nanoscale 2018, 10, 22917–22926. [PubMed: 30499576]

[22]. Suhanovsky MM, Teschke CM, Virology 2015, 479–480, 487–497.

[23]. Jones JA, Giessen TW, Biotechnol. Bioeng. 2020.

[24]. Li W, Nicol F, Szoka FC, Adv. Drug Deliv. Rev. 2004, 56, 967–985. [PubMed: 15066755]

[25]. Kamiyama D, Sekine S, Barsi-Rhyne B, Hu J, Chen B, Gilbert LA, Ishikawa H, Leonetti MD, Marshall WF, Weissman JS, Huang B, Nat. Commun. 2016, 7, 11046; H. Moon, J. Lee, J. Min, S. Kang, Biomacromolecules 2014, 15, 3794–3801. [PubMed: 26988139]

[26]. Panavas T, Sanders C, Butt TR, Methods Mol. Biol. 2009, 497, 303–317. [PubMed: 19107426]

[27]. Romei MG, Boxer SG, Annu. Rev. Biophys. 2019, 48, 19–44. [PubMed: 30786230]

[28]. Ozawa K, Iwasa H, Sasaki N, Kinoshita N, Hiratsuka A, Yokoyama K, Appl. Microbiol. Biotechnol. 2017, 101, 173–183. [PubMed: 27510979]

[29]. Kato C, Kawai E, Shimizu N, Mikekado T, Kimura F, Miyazawa T, Nakagawa K, PLoS One 2018, 13, e0209700. [PubMed: 30576372]

[30]. Lee SY, Lee J, Chang JH, Lee JH, BMB Rep. 2011, 44, 77–86. [PubMed: 21345305]

[31]. Jordan PC, Patterson DP, Saboda KN, Edwards EJ, Miettinen HM, Basu G, Thielges MC, Douglas T, Nat. Chem. 2016, 8, 179–185. [PubMed: 26791902]

[32]. Zhao Z, Fu J, Dhakal S, Johnson-Buck A, Liu M, Zhang T, Woodbury NW, Liu Y, Walter NG, Yan H, Nat. Commun. 2016, 7, 10619. [PubMed: 26861509]

[33]. Edwardson TGW, Tetter S, Hilvert D, Nat. Commun. 2020, 11, 5410; T. G. W. Edwardson, T. Mori, D. Hilvert, J Am. Chem. Soc. 2018, 140, 10439–10442. [PubMed: 33106476]

[34]. Giessen TW, Silver PA, ACS Synth. Biol. 2016, 5, 1497–1504. [PubMed: 27276075]

[35]. Tracey JC, Coronado M, Giessen TW, Lau MCY, Silver PA, Ward BB, Sci. Rep. 2019, 9, 20122; R. M. Putri, C. Allende-Ballestero, D. Luque, R. Klem, K. A. Rousou, A. Liu, C. H. Traulsen, W. F. Rurup, M. S. T. Koay, J. R. Castón, J. J. L. M. Cornelissen, ACS Nano 2017, 11, 12796–12804. [PubMed: 31882935]

[36]. Huang RK, Khayat R, Lee KK, Gertsman I, Duda RL, Hendrix RW, Johnson JE, J. Mol. Biol. 2011, 408, 541–554; R. Rahmanpour, T. D. Bugg, FEBS J 2013, 280, 2097–2104. [PubMed: 21276801]

[37]. Xie Z, Hendrix RW, J. Mol. Biol. 1995, 253, 74–85. [PubMed: 7473718]

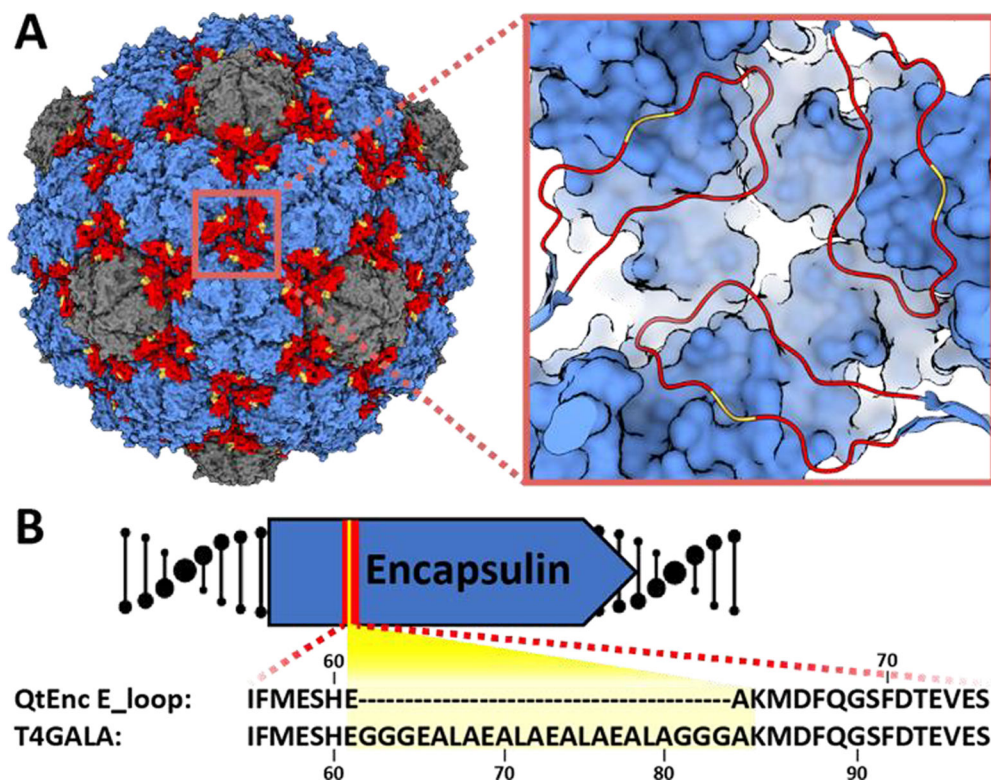[38]. Kim A, Szoka FC, Pharm. Res. 1992, 9, 504–514. [PubMed: 1495896]

Figure 1.
Design of the engineered protein nanocage. A) Surface view of the native *Quasibacillus thermotolerans* T4 encapsulin (QtEnc, PDB 6NJ8), highlighting hexameric (blue) and pentameric (gray) facets, and E-loops (red) along with the GALA peptide insertion site (yellow). Inset: zoomed-in view of the three-fold symmetry axis and insertion site. B) E-loop (red) sequence of QtEnc and T4GALA highlighting the GALA insertion (yellow).
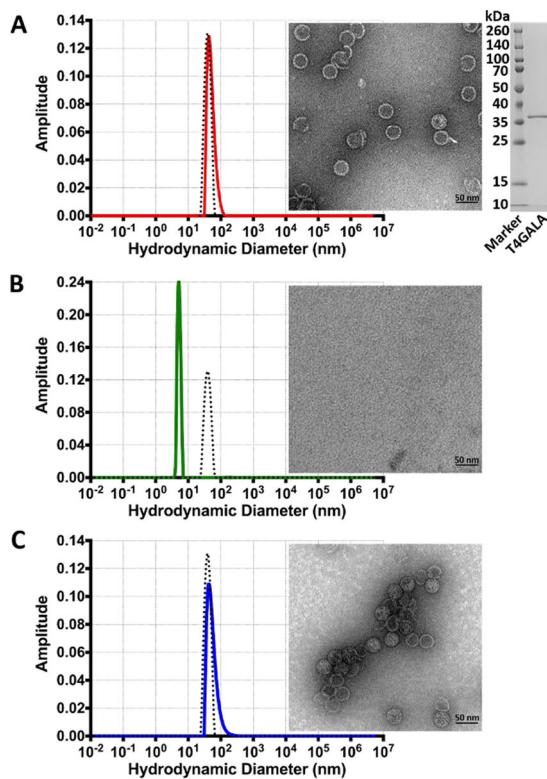
Figure 2.
Assembly, disassembly, and reassembly of the T4GALA protein cage. A) Dynamic light scattering analysis (left) of assembled T4GALA (red) compared to native QtEnc (black dashed) with assembled T4GALA verified via TEM (right). SDS-PAGE analysis of purified T4GALA (far right). B) DLS analysis (left) of disassembled T4GALA after centrifugation (green) with QtEnc reference (black dashed) and disassembled T4GALA TEM analysis (right). C) DLS analysis (left) of reassembled T4GALA (blue) with QtEnc reference (black dashed) and reassembled T4GALA TEM analysis (right). Scale bars: 50 nm.
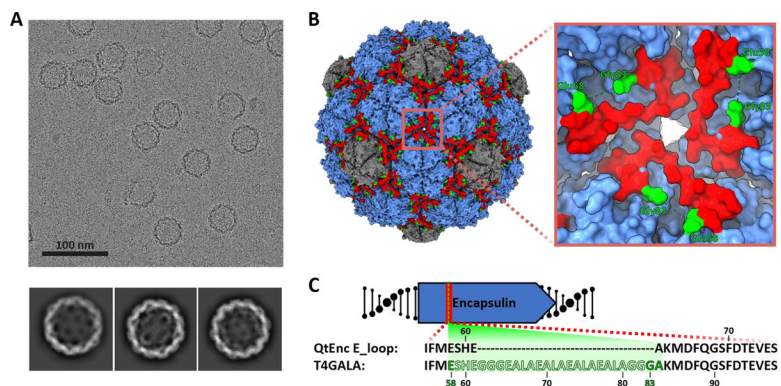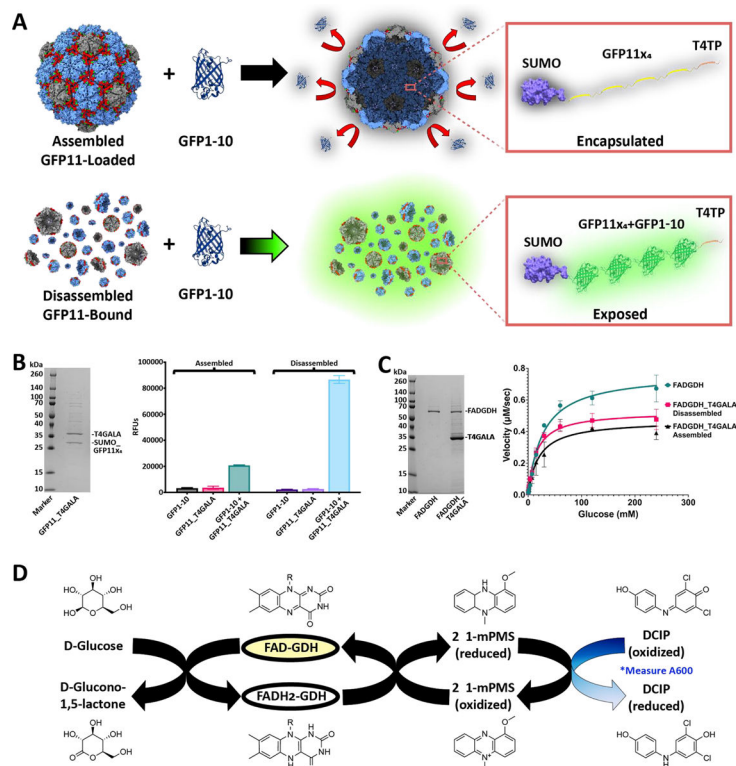
Figure 3.
Structural analysis of T4GALA. A) Representative motion-corrected electron cryomicrograph (top) and 2D class averages of T4GALA. B) Cryo-EM density of T4GALA. Hexameric and pentameric capsomers shown in blue and grey, respectively. E-loops are highlighted in red and the last visible residues flanking the GALA insertion site are shown in green (Glu58 and Gly83). Inset (right) highlighting details of the three-fold symmetry axis to emphasize missing E-loop density (Ser59 to Gly82, green dashes). C) Schematic highlighting the observed (solid) and missing (silhouette) residues in the T4GALA E-loop.

Figure 4.

In vivo cargo loading of T4GALA and characterization of cargo-loaded systems. A) Schematic of split fluorescent protein experiments. Assembled (top) and disassembled (bottom) GFP11×$_4$-loaded/bound T4GALA exposed to the GFP1–10 complement. B) SDS-PAGE analysis of GFP11×$_4$-loaded T4GALA (left). Plate-based fluorescence assays (right) showing increased relative fluorescence for disassembled GFP11×$_4$-bound T4GALA complementation (light blue; right) compared to roughly four-fold lower fluorescence for an equimolar amount of assembled GFP11×$_4$-loaded T4GALA (green, left). C) SDS-PAGE analysis of GDH and GDH-loaded T4GALA (left). Non-linear regression curve with Michaelis-Menten fit of velocity (right) of unencapsulated FAD-dependent glucose dehydrogenase enzyme (green circles), *in vivo* T4GALA-encapsulated enzyme in the disassembled state (pink squares), and *in vivo* T4GALA-encapsulated enzyme in the assembled state (black triangles) with varying concentrations of glucose (two-fold dilutions from 240 mM to 0.94 mM) at a fixed concentration of DCIP (0.07 mM) demonstrating GDH activity. Data are shown as means while error bars represent standard deviations from three independent experiments. D) Schematic summary of the catalyzed enzymatic reaction and the complementary assay measuring the resultant decrease in absorption at 600 nm as DCIP is reduced. FAD, flavin adenine dinucleotide; GDH, glucose dehydrogenase; 1-mPMS, 1-methoxy-5-methylphenazinium methylsulfate; DCIP, 2,6-dichloroindophenol.
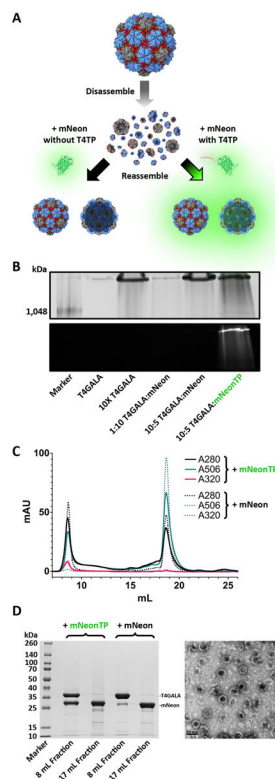
Figure 5.
In vitro cargo loading of T4GALA. A) Schematic of T4GALA *in vitro* cargo loading including protein cage disassembly, *in vitro* loading of targeting peptide-fused cargo (right) and T4GALA reassembly resulting in detectable fluorescence from newly encapsulated mNeon cargo. Conversely, the same procedure is carried out with mNeon lacking the targeting peptide, which fails to result in cargo loading (left) and results in no detectable fluorescence after reassembly. B) NativePAGE analysis showing high molecular weight bands for assembled T4GALA via Coomassie blue staining (top) and fluorescence analysis of mNeon (bottom). C) Size-exclusion chromatography analysis showing *in vitro* cargo loading of targeting peptide-fused mNeon (mNeonTP; absorbance at 506 nm, solid green line) via co-elution with T4GALA as compared to a relative lack of mNeon cargo loading when lacking targeting peptide (dashed lines). D) SDS-PAGE analysis (left) of size-exclusion results for T4GALA with and without mNeon (lanes 2 and 4, respectively; 8 mL fractions from SEC above) and respective excess unencapsulated mNeon (lanes 3 and 5, respectively; 17 mL fractions from SEC above). Corresponding TEM analysis (right) of mNeonTP-loaded T4GALA from preceding SEC (8 mL fraction; lane 2 from SDS-PAGE gel on left). Scale bar: 50 nm.

Table 1.

Encapsulated and unencapsulated GDH enzyme kinetic analyses.

Sample[a]	K_{cat} [95% CI] [b]	$K_m{}^{app}$ [95% CI] [b]	V_{max} [95% CI] [b]
GDH	86.75 s^{-1}	27.68 mM	0.77 μM/sec
	[81.26, 92.71]	[22.56, 33.98]	[0.72, 0.82]
Disassembled	59.33 s^{-1}	15.16 mM	0.53 μM/sec
GDH_T4GALA	[55.99, 62.87]	[12.81, 18.63]	[0.50, 0.56]
Assembled	52.90 s^{-1}	19.83 mM	0.47 μM/sec
GDH_T4GALA	[47.28, 59.17]	[13.63, 28.71]	[0.42, 0.52]

[a]Assays were conducted in triplicate and analyzed via non-linear regression.

[b]Turnover number (kcat), apparent Michaelis-Menten constant ($K_m{}^{app}$) and maximum velocity (V_{max}) were calculated via Michaelis-Menten curve fitting with least square method. CI, confidence interval; GDH, glucose dehydrogenase.